NANO · MICRO small
www.small-journal.com

Highly Sensitive Flexible Tactile Sensors in Wide Sensing Range Enabled by Hierarchical Topography of Biaxially Strained and Capillary-Densified Carbon Nanotube Bundles

*Sangjun Sim, Eunhwan Jo, Yunsung Kang, Euichul Chung, and Jongbaeg Kim**

Flexible tactile sensors with high sensitivity have received considerable attention for their use in wearable electronics, human–machine interfaces, and health-monitoring devices. Although various micro/nanostructured materials are introduced for high-performance tactile sensors, simultaneously obtaining high sensitivity and a wide sensing range remains challenging. Here, a resistive tactile sensor is presented based on the hierarchical topography of carbon nanotubes (CNTs) prepared by a low-cost and straightforward manufacturing process. The 3D hierarchical structure of the CNTs over large areas is formed by transferring vertically aligned CNT bundles to a prestrained elastomer substrate and subsequently densifying them through capillary forming, providing a monotonic increase in the contact area as applied pressure. The deformable and hierarchical structure of CNTs allows the sensor to exhibit a wide sensing range (0–100 kPa), high sensitivity (141.72 kPa^{-1}), and low detection limit (10 Pa). Additionally, the capillary-formed CNT structure results in increased durability of the sensor over repeated pressures. Based on these advantages, meaningful applications of tactile sensors, such as object recognition gloves and multidirectional force perceptions, are successfully realized. Given the scalable fabrication method, 3D hierarchically structured CNTs provide an essential step toward next-generation wearable devices.

1. Introduction

Recently, flexible tactile sensors have been gaining attention for various applications, such as wearable haptic devices, health-monitoring devices, and human–machine interfaces.[1–8] For practical application, flexible tactile sensors should have a high sensitivity (>1 kPa^{-1}) over a wide sensing range (>10 kPa),[9–11] simultaneously prepared with low-cost and scalable fabrications over a large area.[12,13] To satisfy these strict requirements, various sensing principles, which measure the change in electrical signals such as resistance (contact[14]/piezo[15]-resistivity), voltage (piezoelectricity[16]/triboelectricity[17]), and capacitance,[18,19] have been introduced. Among these types, resistive-type tactile sensors, which rely on detecting a change in the contact area with applied pressure, have received significant interest because of their simple signal measurement and easy fabrication.[20–26]

For these contact-resistive-type tactile sensors, surface topographies should be considered significant because they are directly related to performance parameters such as sensitivity, linearity, detection limit, and sensing range. Recently, various microstructured surfaces, such as pyramid,[27,28] pillar,[29,30] and hemisphere[31,32] structures, have been proposed, providing a notable increase in the contact area with respect to the external pressure. Additionally, numerous nanomaterials, including metal nanowires,[33,34] graphene,[35,36] and carbon nanotubes (CNTs),[37,38] have been adopted as conductive sensing materials for sensors with 3D microstructures to enhance the flexibility and sensitivity of tactile sensors. For example, Zhu et al.[39] reported a flexible tactile sensor based on a micropyramid structure with graphene layers. The sensor achieved high sensitivity (−5.53 kPa^{-1}) and ultrafast response (≈0.2 ms). However, the sensing range with high linearity was limited to 0.1 kPa.

Hence, hierarchical structures with a micro-nanotopography are attractive candidates for the sensing materials of tactile sensors. These structures have a large surface area and effective change in the contact area from applied pressure, improving the linearity and sensing range enlargement of the tactile sensors. For example, Bae et al.[40] reported a tactile sensor using a hierarchical microdome structure covered with graphene, where the sensor showed high sensitivity (8.5 kPa^{-1}) with a wide sensing range (0.001–12 kPa). Wang et al.[41] also developed a highly sensitive and stretchable resistive tactile sensor with hierarchically porous structures decorated with conductive carbon black nanoparticles using a 3D printing process. Based on the change in the contact resistance with applied pressure, the sensor showed high sensitivity (5.54 kPa^{-1}) with a wide sensing range (0.01–800 kPa). However, the fabrication of these hierarchical structures demands complicated or time-consuming processes.

This work demonstrates a highly sensitive tactile sensor with a wide sensing range based on a 3D hierarchical structure with CNT bundles as a functional material with a controllable production process. By transferring a prestrained elastomer

S. Sim, E. Jo, Y. Kang, E. Chung, J. Kim
School of Mechanical Engineering
Yonsei University
50-Yonsei Ro, Seodaemun-gu, Seoul 03722, Republic of Korea
E-mail: kimjb@yonsei.ac.kr

The ORCID identification number(s) for the author(s) of this article can be found under https://doi.org/10.1002/smll.202105334.

DOI: 10.1002/smll.202105334

substrate of vertically aligned CNT (VACNT) bundles and subsequently densifying them, we successfully developed a 3D hierarchical structure for the tactile sensor. Although the prestraining technique to make the wrinkled surface was presented various flexible electronics such as strain sensors, tactile sensors, and stretchable electrodes,[42–47] our work is the first study to demonstrate a tactile sensor with a 3D hierarchical structure with CNT bundles through a transfer and densification process. The fabricated sensor achieved remarkable sensing performances with ultrahigh sensitivity (141.72 kPa^{-1} at a pressure range of 0.01–40 kPa) and a wide sensing range (0–100 kPa). In particular, the sensor exhibited high linearity over a wide sensing range (0–40 kPa), while simultaneously maintaining an ultrahigh sensitivity over 100 kPa^{-1}, which is notable considering that it has been challenging to achieve both high sensitivity and a wide sensing range in most of the tactile sensors. The sensor also exhibited a low limit of detection (LOD) (10 Pa), excellent repeatability, durability, and high reproducibility. The sensing performance characterization is further discussed by adjusting the prestrained directions of the elastomer substrate and densification of the VACNT bundles. Furthermore, the potential application of the tactile sensor as a wearable glove for object recognition was presented. In addition, we successfully demonstrated a multidirectional tactile sensor that could distinguish the magnitude and direction of the applied force using structurally designed tactile sensor arrays.

2. Results and Discussion

2.1. Fabrication of the Tactile Sensor

Figure 1a shows the fabrication process of the 3D hierarchical structure with CNT bundles. A silicone elastomer (Ecoflex) substrate was prepared by stretching in the biaxial direction. After that, uncured Ecoflex was spin coated to a constant thickness on the substrate. Then VACNT bundles were synthesized by the chemical vapor deposition (CVD) process on a Si wafer flipped onto the Ecoflex film. After curing the additionally coated Ecoflex, CNT bundles were transferred to the prestrained Ecoflex substrate by contacting and separating them on the flipped wafer (see the Experimental Section for details). Because the adhesion force between the cured Ecoflex and CNT bundles was stronger than that between the Si wafer and CNT bundles,[48] they were transferred entirely to the Ecoflex substrate (Figure S1, Supporting Information, for the photographs of the fabrication process). Figure 1b illustrates a schematic of the tactile sensor based on the 3D hierarchical structure. The sensor consists of a hierarchical structure with CNT bundles and interdigitated electrodes (IDEs) on a flexible printed circuit board, and they are bonded by a polyethylene terephthalate (PET) adhesive film (Figure S2, Supporting Information, for the designed dimension of the sensor). To optimize the thickness of the adhesive film, we analyzed the initial contact resistance

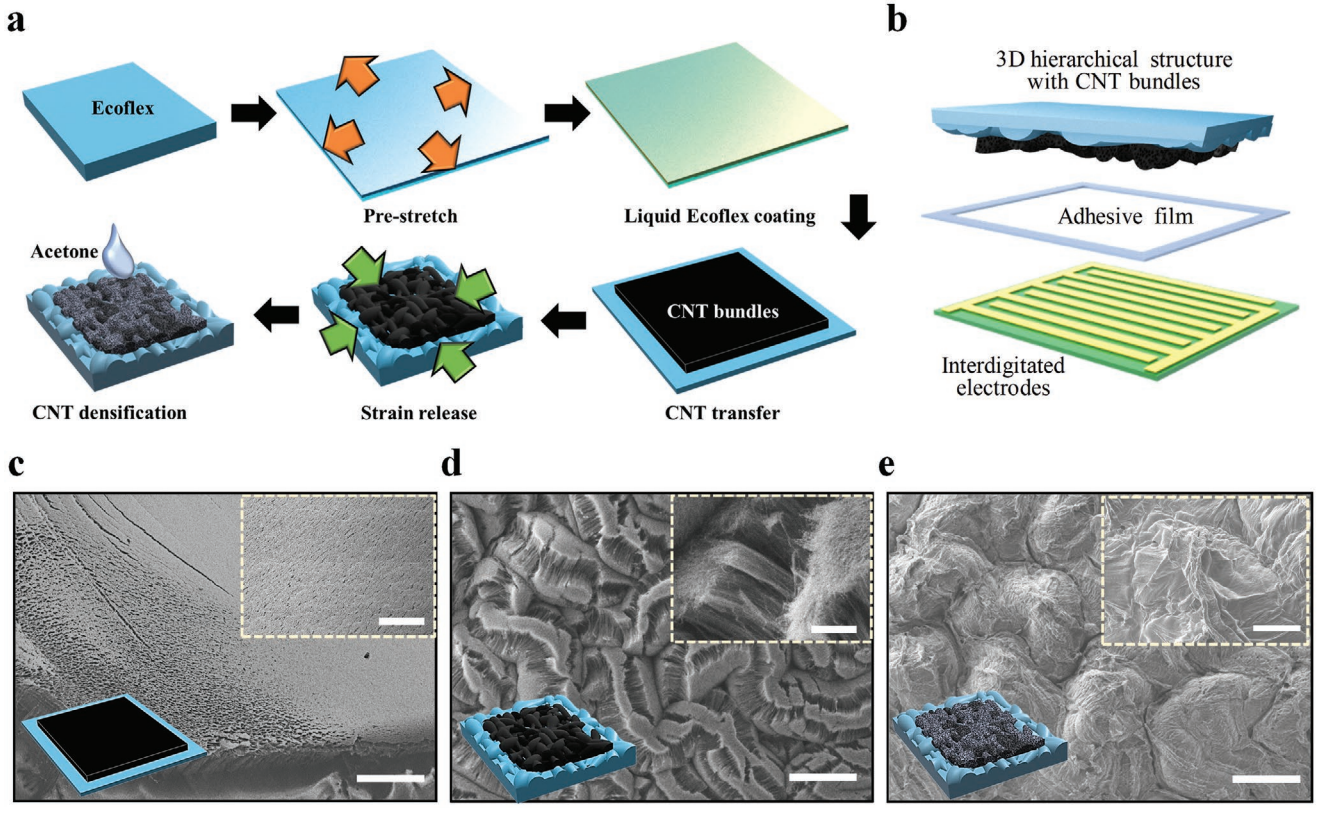

Figure 1. Design and characterization of proposed tactile sensor based on 3D hierarchical structure. Schematics of a) fabrication process for the 3D hierarchical structure with CNT bundles and b) the tactile sensor composed with 3D hierarchical structure, PET adhesive film, and interdigitated electrodes (IDEs). SEM images of c) CNT bundles surface transferred to the Ecoflex substrate, d) CNT bundles of strain released Ecoflex substrate, and e) the 3D hierarchical structure with densified CNT bundles. The scale bars are 500 and 10 µm (inset).

of the sensors with different thicknesses of the adhesive film (Figure S3, Supporting Information).

As shown in the scanning electron microscope (SEM) images in Figure 1c, the VACNT bundles were partially buried in the elastomer as the length of the VACNT bundles (≈300 μm) were longer than the height of the coated film (≈50 μm). After the transfer step, the biaxially prestrained substrate was released to wrinkle the CNT bundles along with the shape of the wrinkled Ecoflex surface. The wrinkled pattern of the surface was successfully formed owing to the difference in the strain direction between the elastomer film and the substrate[45,46] (Figure 1d). The wrinkled CNT structure is not suitable for direct application of a sensing element that utilizes the change in contact resistance owing to its low density and low mechanical stiffness. To increase the stiffness of the CNT bundles, we proceeded to densify the CNT bundles via a "capillary forming" process.[49] As the CNT bundles clumped together, it not only increased the mechanical stiffness but also formed a 3D hierarchical structure on the wrinkled surface (Figure 1e). A comparison of the sensing performance characterization depending on capillary forming would be discussed in Section 2.3.

2.2. Tactile Sensing Performances

The sensing mechanism of the sensor is depicted in **Figure 2**a. The initial state between the 3D hierarchical structure and the electrodes is only partial contact. It has a high contact resistance between CNT hierarchical structure and electrodes and thus a low current value at a bias voltage. When pressure is applied, the contact area between the CNT surface and the electrodes increases, forming more conductive pathways (i.e., increasing the current). In particular, the current increases significantly due to the 3D hierarchical structure, which can easily increase the contact area, inducing the high sensitivity. Additionally, the biaxially wrinkled structure distributes the applied pressure, increasing the contact area even at large pressures.

The sensing performance of the 3D hierarchical structure-based tactile sensor was evaluated with respect to the applied normal pressure (Figure S4, Supporting Information, for the experimental setup). Figure 2b reveals the *I*–*V* curves of the tactile sensor at various pressures (0.5–100 kPa) over applied voltage from −0.1 to 0.1 V. The linear curves indicate the formation of ohmic contact between the CNT surface and IDEs under various pressures and the resistance of the sensor dramatically decreased from 6.6 kΩ to 1.23 Ω when the pressure increased from 0 to 100 kPa. Here, the sensitivity (S) was calculated from the typical definition for the resistive-type tactile sensors, $S = (\Delta I/I_0)/P$, where $\Delta I/I_0$, and P denote the relative change in current and input pressure, respectively. Figure 2c shows the relative current changes ($\Delta I/I_0$) of the 3D hierarchical CNT structure-based tactile sensor under various pressures at a bias voltage of 0.1 V. The measured sensitivities of our sensor were 141.72 and 18.76 kPa^{-1} in the pressure ranges of 0–40 and 40–100 kPa, respectively, showing that the curve is distinguished by two sections, a more sensitive region (0–40 kPa) and relatively less sensitive region (40–100 kPa). Previous studies on contact-resistive type tactile sensors with microstructures have similarly revealed two or more distinguished sensitivity sections.[23,30] The contact area between the electrodes and the functional materials increased with applied pressure, but there was a difference in the level of change in the contact area.[24] Nevertheless, it is notable that our hierarchical CNT-based tactile sensor shows high sensitivity (141.72 kPa^{-1}) while maintaining high linearity (correlation coefficient: 0.983) over a wide sensing range (0–40 kPa).

Figure 2d compares the sensitivity and pressure-sensing range of the proposed sensor and the recently published flexible tactile sensors (see Table S1, Supporting Information, for the specific values of the sensors). Our tactile sensor exhibits a higher sensitivity than most of the other sensors reported.[12,13,20–25,50,51] Some sensors showed higher sensitivity than ours, but the range was limited to below 10 kPa,[22,24] which limits the application. Our sensor simultaneously exhibits high sensitivity and a wide range of detectable pressure, owing to the CNT bundles-based 3D hierarchical structure inducing a significant change in the contact area and dispersing the applied pressure. Furthermore, the fabrication process, based on prestretching and transfer processes, is cost-effective and straightforward.

As shown in Figure 2e, the dynamic response of the tactile sensor is stable even when loading/unloading cyclic pressures of 10, 20, and 30 kPa were applied. Furthermore, we investigated the response and recovery times of the sensor by applying a pressure of 5 kPa (Figure 2f), which were 102 and 82 ms, respectively. We also have investigated a response and recovery time for a higher pressure of 10 and 20 kPa, as shown in Figure S5 in the Supporting Information. Although these response times (141 and 244 ms, respectively) and recovery times (114 and 152 ms, respectively) are longer than that for the lower pressure (5 kPa) applied the results are still comparable to those of the previously reported tactile sensors.[50,52] Therefore, these results show that our sensor is suitable for use in various applications such as real-time health monitoring devices and tactile feedback smart gloves.[41,53] The LOD of our sensor was measured as 10 Pa (Figure S6, Supporting Information), and this small value can be attributed to the presence of a 3D hierarchical structure. The contact area between the hierarchical structure and electrodes easily increased, even if subtle pressure is applied to the sensor. We confirmed that our sensor could detect low and high pressures, ranging from 10 Pa to 100 kPa. We also evaluated the repeatability of the sensor by applying a 1000 cycles loading-unloading test at 100 kPa. As shown in Figure 2g, there was no significant degradation in the sensing performance, including the sensitivity and linearity in the detection ranges, which revealed only a variation of 5.9% over 1000 cyclic loading tests. We also have observed the repeated pressure loading test for 18 000 cycles by applying 20 kPa to the sensor. As shown in Figure S7 in the Supporting Information, the response of the sensor has observed no significant change in current, and this result confirmed the stability and durability of the sensor. The high durability of our sensor originates from using a contact material as densified carbon nanotube bundles, with high mechanical robustness.[49] It was confirmed that the sensor has sufficient durability compared to other reported tactile sensors.[54,55] These results indicate that the possible damage of the morphology of the hierarchical CNT surface was minimal after the application of repeated pressure.

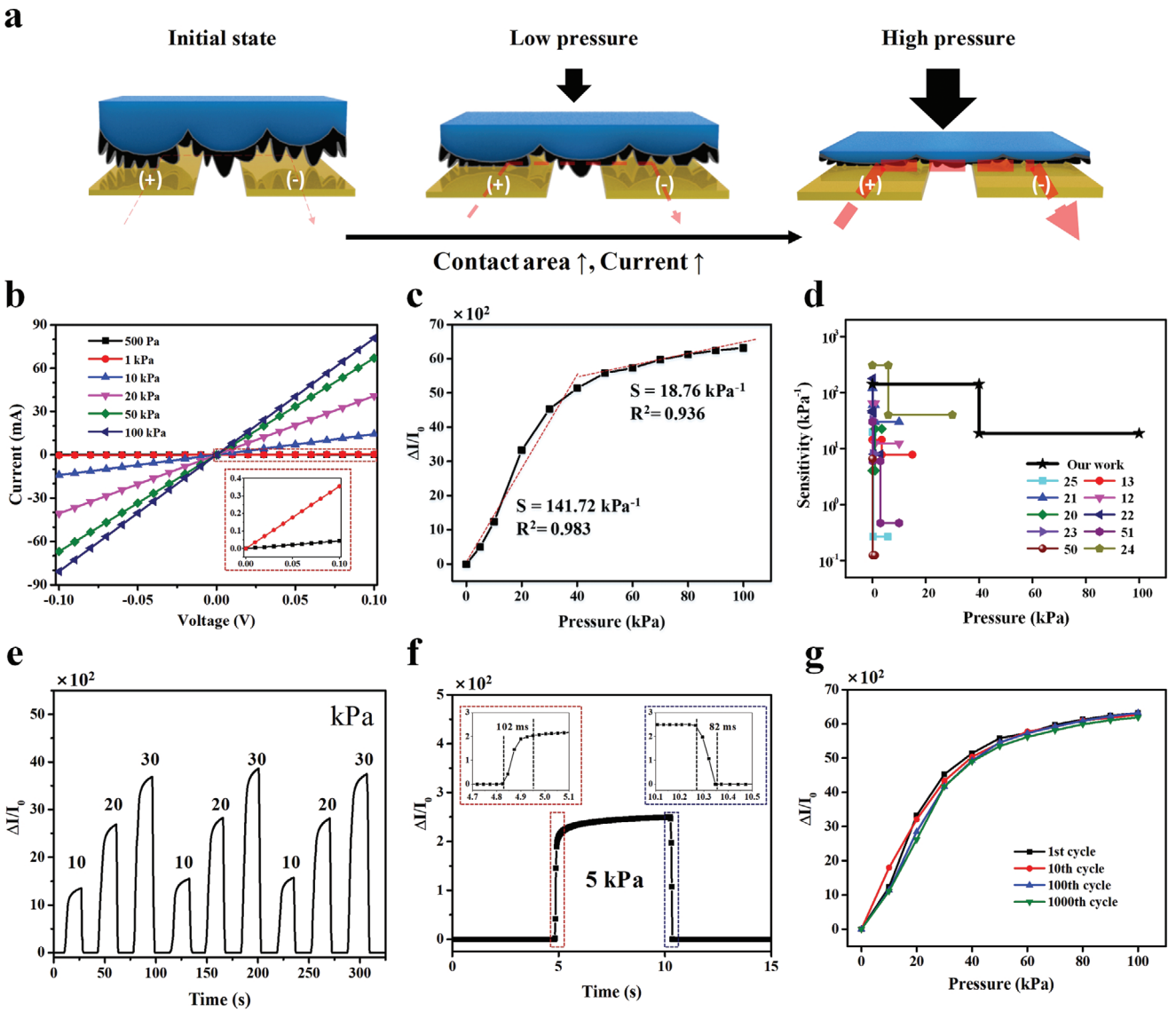

Figure 2. Sensing performances of the 3D hierarchical structure-based tactile sensor under a normal pressure. a) Schematic illustration of the sensing mechanism of our sensor under applied pressure. The contact area between the conductive 3D hierarchical structure and electrodes increases, thereby increasing current. b) Current–voltage curves of the sensor under various static pressure (0.5–100 kPa). c) Normalized change in current of the sensor under the pressures ranging from 0 to 100 kPa. d) Comparison of sensitivity and sensing range of recently reported tactile sensors and our tactile sensor. e) Dynamic responses of the tactile sensor to various pressures of 10, 20, and 30 kPa. f) Response and recovery times of the sensor for a loading/unloading cycle from 0 to 5 kPa. g) Normalized current changes of the sensor under repetitive loading cycles. The results are compared to the 1st, 10th, 100th, and 1000th cycle.

We conducted a pressure-sensing test with three identically designed sensors to verify their reproducibility (Figure S8, Supporting Information). Although a slight deviation of sensor output was observed to be about 17.3%, all the sensors exhibited a high sensitivity of 100 kPa^{-1} in the wide sensing range of 0–40 kPa.

2.3. Characterization of the Sensing Performance

To demonstrate the effect of wrinkling direction on the surface, we transferred the VACNT bundles to the Ecoflex substrate stretched to 150% of the original length in different directions (uniaxially prestrained, bi-axially prestrained, and unstrained). We performed the CNT densification process under the same conditions in all cases. As shown in **Figure 3**a, the sensors were tested by measuring the relative current changes under various applied pressures. The sensitivities of the unstrained, uniaxially prestrained, and bi-axially prestrained sensors were 0.69, 54.13, and 141.72 kPa^{-1}, respectively (Figure S9, Supporting Information, for SEM images of fabricated CNT bundles with the different wrinkled shape).

The sensor with CNT bundles on the unstrained Ecoflex substrate showed a low sensitivity (0.69 kPa^{-1} in a pressure

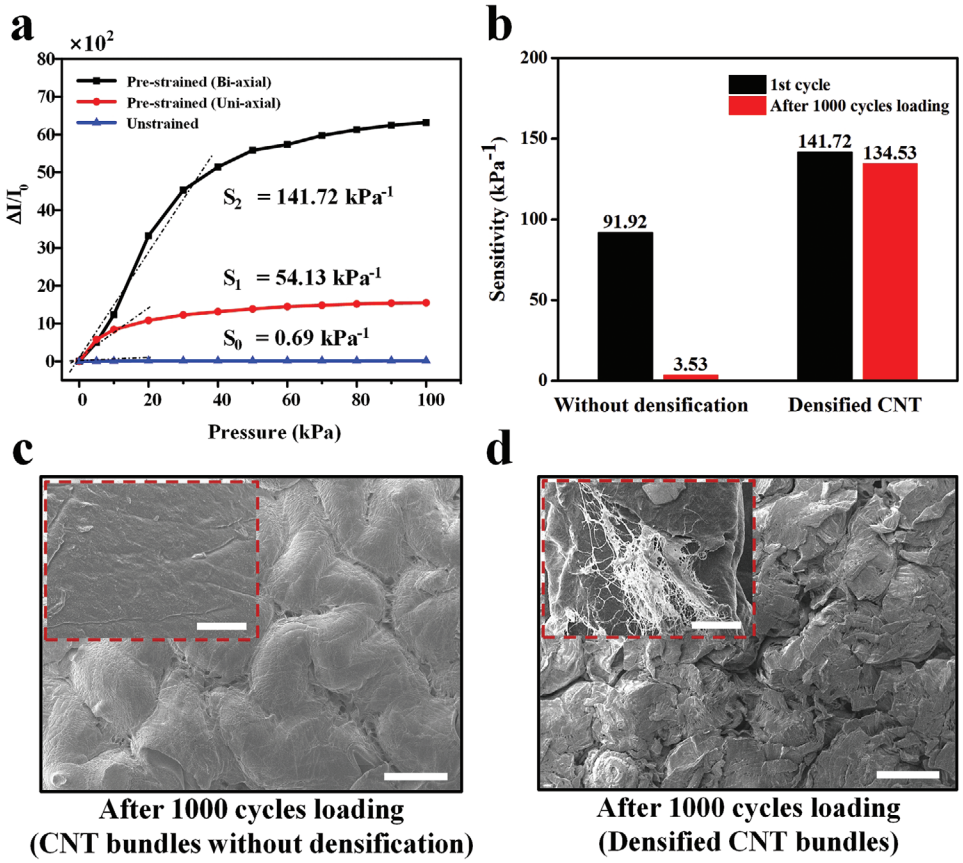

Figure 3. Pressure-responses studies of the sensors with different topographies composed of CNT bundles. a) Normalized current changes the sensors under applied pressure. The sensors are fabricated with different initial prestrain orientations (biaxial, uniaxial, and unstrained). b) Sensitivities of the sensors with densified CNT bundles and CNT bundles without densification at the 1st and after 1000 cycles loading. c,d) SEM images of the CNT bundle structures after 1000 cycles loading. The scale bars are 500 and 10 μm (inset).

range of 0–20 kPa) because the initial contact area between the electrodes and the CNT surface was large. When the pressure was applied, the sensor without the wrinkled structure had a limited sensing range. However, the sensitivity of the sensor with the CNT surface using the uniaxially prestrained substrate was 54.13 kPa^{-1} in a pressure range of 0–20 kPa, which was nearly 80 times higher than that of the unstrained substrate. This could be attributed to the presence of the wrinkled elastomer and densified VACNT bundles, whose area of contact with the electrode changed sensitively even at low pressures. Furthermore, the CNT surface using the bi-axially prestrained Ecoflex substrate showed higher sensitivity than the other sensors. For the densified CNT bundles formed along with the bi-axially wrinkled elastomer, the sensitivity is 141.72 kPa^{-1} in a wide pressure range of 0–40 kPa. These results confirm that the 3D hierarchical structure with CNT bundles induces a significant change in the contact area, thereby increasing the sensitivity of the tactile sensor. We have fabricated the sensors with the different prestrain of 50%, 150%, and 250%, and analyzed the change in current of the sensors (Figure S10, Supporting Information, for SEM images of fabricated tactile sensors with the different prestrain of 50%, 150%, and 250%). The sensitivities of the sensor with 50%, 150%, and 250% prestrained elastomer substrate showed 119.99, 141.72, and 111.08 kPa^{-1}, respectively in the pressure range of 0–40, and 26.53, 18.76, and 34.43 kPa^{-1}, respectively in the pressure range 40–100 kPa (Figure S11, Supporting Information). Although a slight difference in sensitivity exists for the three sensors, all the sensors show high sensitivity and a wide sensing range compared to reported other tactile sensors.[12,20,25]

Moreover, to verify the effect of the capillary forming process for enhancing the durability of the sensor, we fabricated a sensor using the structure without the densification process of CNT bundles, and the other procedures were the same. As previously mentioned, the mechanical stiffness of the CNT bundles increased through the capillary forming process, which densifies the CNT bundles.[49] The surface without densification of the CNT bundles also had a large surface area, as shown in Figure 1e. The fabricated sensor using this surface had a high sensitivity (91.92 kPa^{-1}), because the porous VACNT bundle structure caused a significant change in the surface area at low pressure. However, the highly sensitive pressure range was limited to 0–10 kPa (Figure S12, Supporting Information, for pressure-sensing performance). As shown in Figure 3b, the CNT-based sensor without densification process, which has not been capillary formed, showed a drastic decrease in sensitivity after applying repeated pressure for 1000 cycles. The sensitivity after 1000 cycles of loading in a pressure range of 0–100 kPa

was 3.53 kPa^{-1}, which is a 96.2% decrease from the 1st cycle. Figure 3c shows that the CNT surface without densification after the loading test did not retain the initial shape of the porous CNT structure. However, the sensor using the capillary-formed CNT surface exhibited excellent repeatability, as shown in Figure 3b. The sensitivity of the sensor was maintained even after 1000 cycles of the loading test, and only a slight decrease of 5.1% was observed. Figure 3d shows that the 3D hierarchical structure with CNT bundles after cyclic loading was maintained, owing to enhancement of mechanical stiffness.

To investigate the effect of CNT length on sensor performances, we fabricated the three tactile sensors with different lengths (30, 120, and 300 µm) of CNT bundles and characterized the pressure sensing performances. The length of CNT has been adjusted by controlling the reaction time for flowing acetylene gas (C_2H_2) during the CVD process for CNT synthesis.[56] As shown in Figure S13a,b in the Supporting Information, the measured sensitivities of the tactile sensors with CNT lengths of 30, 120, and 300 µm (as presented in Figure 2c) were 11.75, 134.32, and 141.72 kPa^{-1}, respectively. In the case of the sensor with CNT length of 30 µm (i.e., shorter than the thickness of the coated elastomer), there is no hierarchical structure because the transferred CNT bundles were completely embedded in the elastomer, resulting in the relatively low sensitivity (11.75 kPa^{-1}) (Figure S13c, Supporting Information). On the other hand, the tactile sensor with CNT length of 120 µm (i.e., longer than the thickness of the coated elastomer) has a high sensitivity (134.32 kPa^{-1}). The CNT bundles are transferred to the elastomer with only partially embedded and exposed CNT bundles enable to form a hierarchical structure with subsequent densification process (Figure S13d, Supporting Information). We could confirm that the sensitivity is not significantly affected by the length of CNTs if the CNTs are long enough to form a hierarchical structure.

We verified that our sensor exhibits high sensitivity and a wide sensing range due to the 3D hierarchical structure with CNT bundles that easily increases the contact area at the applied pressure and continuously increases the contact area even at large pressures. Additionally, it is confirmed that densified CNT bundles on the wrinkled elastomer enabled to improve mechanical stiffness, satisfying the durability of the sensor.

2.4. Application in Wearable Tactile Glove

Our tactile sensor with flexibility and high sensitivity is a promising candidate for use in sophisticated wearable devices such as teleoperated surgery and virtual reality system.[57,58] In particular, our sensor also has an advantage of a wide sensing range, which is meaningful in recognizing various pressures that have been difficult with conventional tactile gloves. To demonstrate the feasibility of our sensor as a wearable device, we developed a wearable tactile glove that can detect various types of tactile information; a photograph of the fabricated device is shown in **Figure 4**a. The device consists of five tactile sensors based on the hierarchical structure with CNT bundles, attached to the fingertips of a commercial knit glove. To verify the ability of the tactile glove, we measured the five sensor signals while grasping or squeezing a rubber blower (Figure 4b). As shown

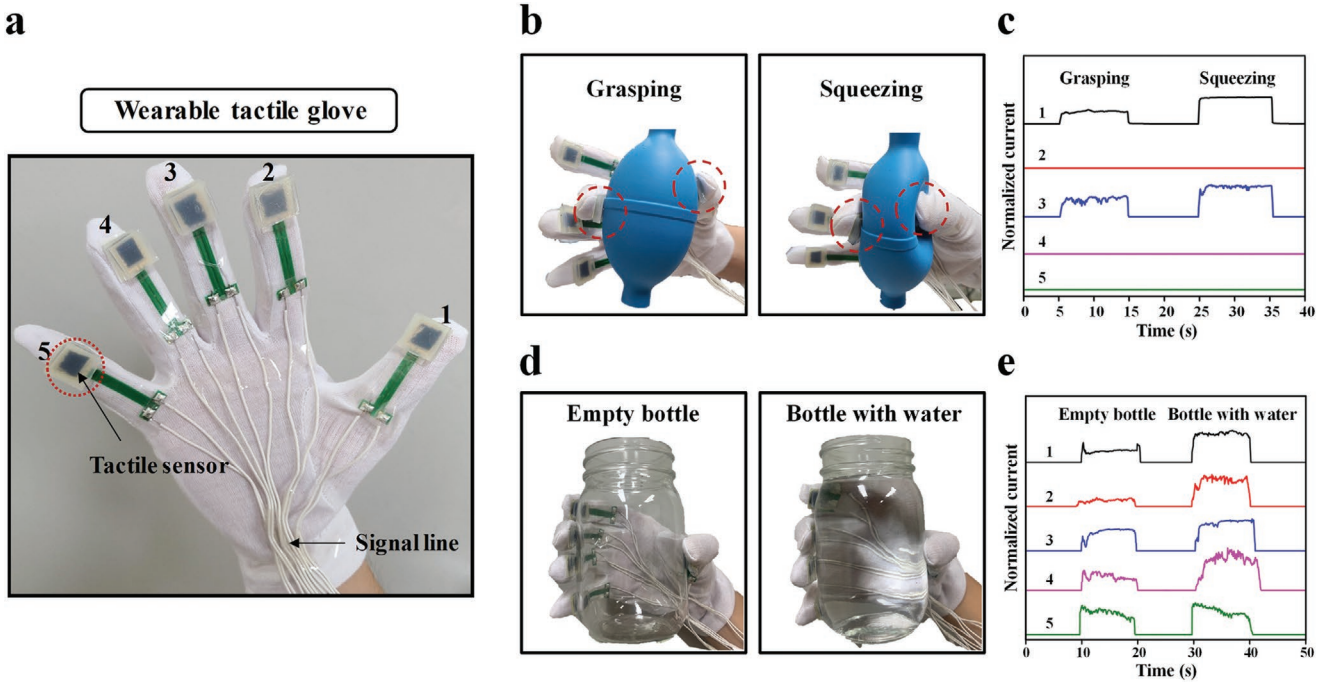

Figure 4. Demonstration of wearable tactile glove with 3D hierarchical structure-based tactile sensor. a) Photograph of the tactile glove based on the tactile sensors with 3D hierarchical structure with CNT bundles. b) Photographs of a user wearing tactile glove holding on an air blower, grasping or squeezing. c) Responses of the tactile sensors of each finger when holding the air blow. d) Photographs of holding on an empty bottle and bottle with water. e) Responses of the tactile sensors of each finger when holding up the bottle.

in Figure 4c, the glove could distinguish differently applied pressure from different motions, for example, the pressure of squeezing the blower was greater than the pressure of grasping it. Furthermore, we also verified that the light and heavy objects were discerned by measuring the pressure applied to the sensors of the tactile glove (Figure 4d,e). When the user held an empty bottle (250 g), the current values of the five sensors changed relatively little, while holding the bottle filled with water (650 g) resulted in a larger change in current. It was confirmed that the sensing responses of holding a heavy object are higher than those of grasping a light object because different amounts of normal force should be applied to the object of different weights to prevent slipping. This result indicates that our sensor may possibly be applied for the force control of robotic manipulators.

2.5. Demonstration of Multidirectional Sensing

We demonstrated a multidirectional tactile sensor using four sensing cells to distinguish the magnitude and direction of the applied force. Each sensing cell is comprised of a hierarchical structure based on CNT bundles and a set of IDEs bonded to it (**Figure 5**a). The hierarchical surface with CNT bundles of a multidirectional tactile sensor was fabricated by transferring the VACNT bundles divided into four regions to a single

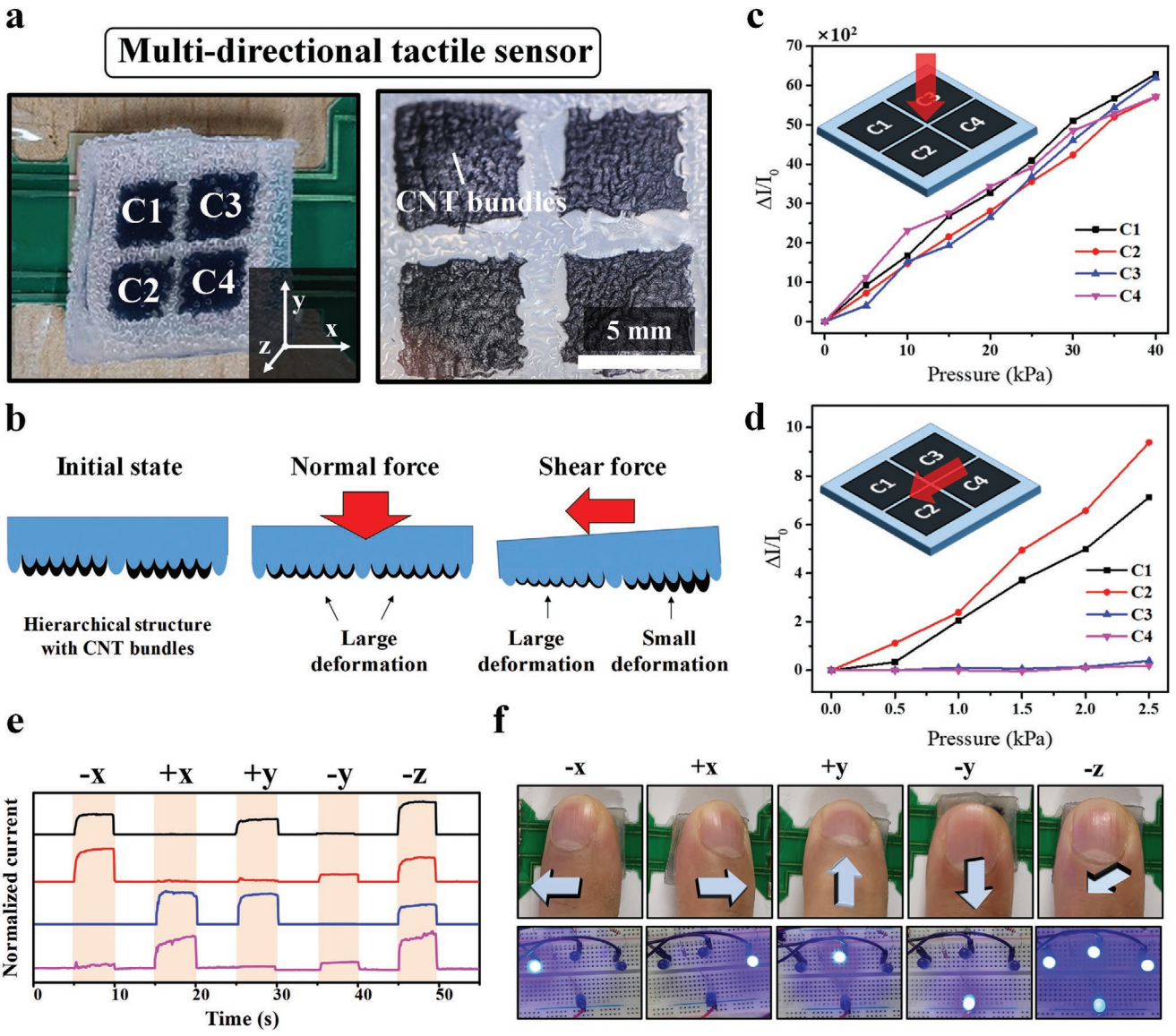

Figure 5. Demonstration of the tactile sensor capable of multidirectional sensing. a) Photographs of tactile sensor and 3D hierarchical structure with CNT bundles divided into four cells. b) Sensing mechanism of the multidirectional tactile sensor when a normal or shear force is applied. c) Normalized change in current of each cell under different normal pressures ranging from 0 to 40 kPa. d) Normalized change in current of each cell under different shear pressure ranging from 0 to 2.5 kPa. e) Dynamic responses of the tactile sensor when multiple direction pressures are applied to the sensor. f) Dynamic changes in the LED arrays when multidirectional pressure is applied to the sensor.

elastomer substrate (Figure S14, Supporting Information). The sensing mechanism of the sensor is shown in Figure 5b. When a normal force was applied to the sensor, the four cells were pressed simultaneously, inducing a similar change in current because of the decrease in the contact resistance. On the other hand, when a shear force was applied, the amount of change in current was larger in the cells located in the direction of the force as the contact area increases. For example, in Figure 5a, when a shear force was applied in the $+x$ direction, a larger change in current was observed in sensing cell 1 (C1) and 2 (C2), while a small change was shown in the other two cells. To verify the multidirectional sensing capability, the current change in each of the four cells was measured simultaneously by applying normal and shear forces to the sensor (Figure 5c,d). For a normal force applied, the current increased in each cell, and the sensors showed a high sensitivity (≈150 kPa^{-1} in a pressure range of 0–40 kPa). This is very close to the sensitivity of the single cell (S = 141.72 kPa^{-1}) tested earlier, because each cell of the multidirectional sensor is identical to the single cell with the 3D hierarchical structure with CNT bundles. As shown in Figure 5d, when a shear force was applied, the cells C1 and C2 undergo a large deformation and showed a sensitivity of ≈3.5 kPa^{-1} in a pressure range of 0–2.5 kPa. This sensitivity value was more than 30 times higher than that of the other two cells C3 and C4 with a small deformation.

To distinguish the direction of the multiple forces, we demonstrated a device that turns on the light in the direction of applied force. The device consists of a multidirectional tactile sensor, four light-emitting diodes (LEDs), and a microcontroller unit for connecting them (Figure S15, Supporting Information, for the detailed configuration of the device). When the force was applied in different directions, we measured the signals of the four sensing cells (Figure 5e). When the normalized current change ($\Delta I/I_0$) was more than 10 for both cells in the direction of the applied force, the light in that direction was turned on (Figure 5f). For example, when a $+x$ direction shear force was applied, the light on the right was turned on, and when a normal force was applied, all the lights were turned on. This demonstration reveals that our sensors can be utilized in tactile interface systems that require high sensitivity and multidirectional sensing.

3. Conclusion

We have developed a tactile sensor based on a 3D hierarchical structure with CNT bundles, possessing ultrahigh sensitivity and a wide pressure-sensing range. The structure is fabricated by transferring CNT bundles onto a prestrained elastomer substrate and densifying them. The 3D hierarchical structure results in a sharp increase in the contact area between the IDEs and the CNT bundles as pressure is applied. Furthermore, the bi-axially wrinkled structure can efficiently distribute the pressure, extending a pressure sensing range. The topography of the densified VACNT structure with enhanced mechanical stiffness is maintained under repeated loading at high pressure, improving durability of the sensor. The characterization of the sensing performance is experimentally confirmed by adjusting the surface shape through a controllable fabrication process. The sensor exhibits excellent sensing performance with high sensitivity (141.72 kPa^{-1} in a pressure range of 0.01–40 kPa) and a wide sensing range (0.01–100 kPa) as well as high repeatability and reproducibility. In addition, we have successfully demonstrated object recognition using a wearable tactile glove with 3D hierarchical structure-based tactile sensors. Furthermore, a device distinguishing normal/shear forces is demonstrated using CNT bundles divided into four cells. With the 3D hierarchical structure comprising CNT bundles with a large surface area and high mechanical stiffness, the proposed tactile sensor will be promising for various applications, such as wearable haptic devices and health-monitoring systems.

4. Experimental Section

Synthesis of VACNT Bundles: The Si substrate was prepared by dicing a bare Si wafer. A 2 nm thick iron catalyst was deposited on a Si substrate using a sputtering system (108 Auto Sputter Coater, Cressington Scientific Instruments). VACNT bundles were synthesized at the catalyst sites via the CVD process. First, the catalyst-coated Si wafer was loaded into a vacuum chamber with a furnace (TF55030C-1, Thermo Scientific). The sample was heated to 720 °C in a furnace with a flow of 100 sccm of nitrogen (N_2). When the temperature stabilized, the gas was changed to 100 sccm of ammonia (NH_3) for pretreatment. After 30 min of ammonia flow, acetylene (C_2H_2) as a precursor flowed to the sample for 15 min to synthesize the CNT bundles.

Fabrication of 3D Hierarchical Structure with CNT Bundles: A 2 mm thick silicone elastomer substrate was prepared by mixing part A and part B of Ecoflex (00–30, Smooth-On Inc.) at a 1:1 ratio by weight and degassing in a vacuum chamber for 5 min. The Ecoflex mixture was poured into a petri dish and cured at 80 °C for 30 min. Next, the cured elastomer film was prestretched and fixed in bi-axial directions. After stretching, the liquid Ecoflex mixture was spin coated on the stretched film to a thickness of 50 µm, and the Si substrate with the synthesized VACNT bundles was flipped and attached to the Ecoflex coated film. The VACNT bundles were transferred to the elastomer by curing the Ecoflex film and removing the Si substrate. After the transfer process, the prestretched Ecoflex film released the strain to create a wrinkled structure with CNT bundles. Finally, acetone was dropped on the CNT bundles and dried at 80 °C for 5 min, densifying the VACNT bundles.[49] The VACNT bundles have a high aspect ratio and porous structure, and the shape of the VACNTs can be controlled by the densification process.[59] Using these characteristics of VACNT, a tactile sensor was fabricated with hierarchical structures, inducing high sensitivity and a wide sensing range. The VACNT bundles are transferred to the elastomer as only a partially embedded state, and thus the exposed VACNT bundles allow the formation of a hierarchical structure through a subsequent densification process.

Device Characterization: The 3D hierarchical morphologies containing CNT bundles were investigated using SEM (IT-500HR, JEOL). To estimate the pressure-sensing performance, such as sensitivity and sensing range, pressure was applied and measured using a force measuring device (DTG-1, DigiTech) installed on a vertical push–pull control machine (KMX-1000N, MAS UTM). Simultaneously, the change in the current of the sensors was measured using a sourcemeter (2614B, Keithley).

Supporting Information

Supporting Information is available from the Wiley Online Library or from the author.

Acknowledgements

This work was supported by the National Research Foundation of Korea(NRF) grant funded by the Korea government(MSIT) (No. 2021R1A2B5B03002850).

Conflict of Interest

The authors declare no conflict of interest.

Data Availability Statement

Research data are not shared.

Keywords

carbon nanotubes, hierarchical structures, tactile sensors, wide sensing range

Received: September 2, 2021
Revised: September 30, 2021
Published online:

[1] J. C. Yang, J. Mun, S. Y. Kwon, S. Park, Z. Bao, S. Park, *Adv. Mater.* **2019**, *31*, 1904765.
[2] R. Yin, D. Wang, S. Zhao, Z. Lou, G. Shen, *Adv. Funct. Mater.* **2020**, *31*, 2008936.
[3] Z. Li, S. Zhang, Y. Chen, H. Ling, L. Zhao, G. Luo, X. Wang, M. C. Hartel, H. Liu, Y. Xue, R. Haghniaz, K. J. Lee, W. Sun, H. J. Kim, J. Lee, Y. Zhao, Y. Zhao, S. Emaminejad, S. Ahadian, N. Ashammakhi, M. R. Dokmeci, Z. Jiang, A. Khademhosseini, *Adv. Funct. Mater.* **2020**, *30*, 2003601.
[4] N. Luo, Y. Huang, J. Liu, S. C. Chen, C. P. Wong, N. Zhao, *Adv. Mater.* **2017**, *29*, 1702675.
[5] Y. Pang, H. Tian, L. Tao, Y. Li, X. Wang, N. Deng, Y. Yang, T. L. Ren, *ACS Appl. Mater. Interfaces* **2016**, *8*, 26458.
[6] S. Lee, S. Franklin, F. A. Hassani, T. Yokota, M. O. G. Nayeem, Y. Wang, R. Leib, G. Cheng, D. W. Franklin, T. Someya, *Science* **2020**, *370*, 966.
[7] S. Lee, A. Reuveny, J. Reeder, S. Lee, H. Jin, Q. Liu, T. Yokota, T. Sekitani, T. Isoyama, Y. Abe, Z. Suo, T. Someya, *Nat. Nanotechnol.* **2016**, *11*, 472.
[8] T. Someya, T. Sekitani, S. Iba, Y. Kato, H. Kawaguchi, T. Sakurai, *Proc. Natl. Acad. Sci. U. S. A.* **2004**, *101*, 9966.
[9] Y. Huang, Y. Chen, X. Fan, N. Luo, S. Zhou, S. C. Chen, N. Zhao, C. P. Wong, *Small* **2018**, *14*, 1801520.
[10] L. Q. Tao, K. N. Zhang, H. Tian, Y. Liu, D. Y. Wang, Y. Q. Chen, Y. Yang, T. L. Ren, *ACS Nano* **2017**, *11*, 8790.
[11] K. Sun, H. Ko, H. H. Park, M. Seong, S. H. Lee, H. Yi, H. W. Park, T. il Kim, C. Pang, H. E. Jeong, *Small* **2018**, *14*, 1803411.
[12] Q. J. Sun, J. Zhuang, S. Venkatesh, Y. Zhou, S. T. Han, W. Wu, K. W. Kong, W. J. Li, X. Chen, R. K. Y. Li, V. A. L. Roy, *ACS Appl. Mater. Interfaces* **2018**, *10*, 4086.
[13] M. Liu, X. Pu, C. Jiang, T. Liu, X. Huang, L. Chen, C. Du, J. Sun, W. Hu, Z. L. Wang, *Adv. Mater.* **2017**, *29*, 1703700.
[14] Y. Lee, J. Park, S. Cho, Y. E. Shin, H. Lee, J. Kim, J. Myoung, S. Cho, S. Kang, C. Baig, H. Ko, *ACS Nano* **2018**, *12*, 4045.
[15] N. Luo, W. Dai, C. Li, Z. Zhou, L. Lu, C. C. Y. Poon, S. C. Chen, Y. Zhang, N. Zhao, *Adv. Funct. Mater.* **2016**, *26*, 1178.
[16] J. Jiang, S. Tu, R. Fu, J. Li, F. Hu, B. Yan, Y. Gu, S. Chen, *ACS Appl. Mater. Interfaces* **2020**, *12*, 33989.
[17] Y. Jiang, K. Dong, X. Li, J. An, D. Wu, X. Peng, J. Yi, C. Ning, R. Cheng, P. Yu, Z. L. Wang, *Adv. Funct. Mater.* **2020**, *31*, 2005584.
[18] S. R. A. Ruth, L. Beker, H. Tran, V. R. Feig, N. Matsuhisa, Z. Bao, *Adv. Funct. Mater.* **2020**, *30*, 1903100.
[19] H. B. Choi, J. Oh, Y. Kim, M. Pyatykh, J. C. Yang, S. Ryu, S. Park, *ACS Appl. Mater. Interfaces* **2020**, *12*, 16691.
[20] Y. Ma, Y. Yue, H. Zhang, F. Cheng, W. Zhao, J. Rao, S. Luo, J. Wang, X. Jiang, Z. Liu, N. Liu, Y. Gao, *ACS Nano* **2018**, *12*, 3209.
[21] B. Yin, X. Liu, H. Gao, T. Fu, J. Yao, *Nat. Commun.* **2018**, *9*, 5161.
[22] B. Zou, Y. Chen, Y. Liu, R. Xie, Q. Du, T. Zhang, Y. Shen, B. Zheng, S. Li, J. Wu, W. Zhang, W. Huang, X. Huang, F. Huo, *Adv. Sci.* **2019**, *6*, 1801283.
[23] J. Jia, G. Huang, J. Deng, K. Pan, *Nanoscale* **2019**, *11*, 4258.
[24] K. Zhou, C. Zhang, Z. Xiong, H. Y. Chen, T. Li, G. Ding, B. Yang, Q. Liao, Y. Zhou, S. T. Han, *Adv. Funct. Mater.* **2020**, *30*, 2001296.
[25] M. Jian, K. Xia, Q. Wang, Z. Yin, H. Wang, C. Wang, H. Xie, M. Zhang, Y. Zhang, *Adv. Funct. Mater.* **2017**, *27*, 1606066.
[26] X. Tang, C. Wu, L. Gan, T. Zhang, T. Zhou, J. Huang, H. Wang, C. Xie, D. Zeng, *Small* **2019**, *15*, 1804559.
[27] B. Zhu, H. Wang, Y. Liu, D. Qi, Z. Liu, H. Wang, J. Yu, M. Sherburne, Z. Wang, X. Chen, *Adv. Mater.* **2016**, *28*, 1559.
[28] C. Ma, D. Xu, Y.-C. Huang, P. Wang, J. Huang, J. Zhou, W. Liu, S.-T. Li, Y. Huang, X. Duan, *ACS Nano* **2020**, *14*, 12866.
[29] C. Jeong, H. Ko, H. T. Kim, K. Sun, T. H. Kwon, H. E. Jeong, Y. Bin Park, *ACS Appl. Mater. Interfaces* **2020**, *12*, 18813.
[30] J. Park, J. Kim, J. Hong, H. Lee, Y. Lee, S. Cho, S. W. Kim, J. J. Kim, S. Y. Kim, H. Ko, *NPG Asia Mater* **2018**, *10*, 163.
[31] D. Lee, J. Kim, H. Kim, H. Heo, K. Park, Y. Lee, *Nanoscale* **2018**, *10*, 18812.
[32] J. Park, Y. Lee, J. Hong, M. Ha, Y. Do Jung, H. Lim, S. Y. Kim, H. Ko, *ACS Nano* **2014**, *8*, 4689.
[33] B. Zhu, Y. Ling, L. W. Yap, M. Yang, F. Lin, S. Gong, Y. Wang, T. An, Y. Zhao, W. Cheng, *ACS Appl. Mater. Interfaces* **2019**, *11*, 29014.
[34] S. Gong, W. Schwalb, Y. Wang, Y. Chen, Y. Tang, J. Si, B. Shirinzadeh, W. Cheng, *Nat. Commun.* **2014**, *5*, 3132.
[35] W. Chen, X. Gui, B. Liang, R. Yang, Y. Zheng, C. Zhao, X. Li, H. Zhu, Z. Tang, *ACS Appl. Mater. Interfaces* **2017**, *9*, 24111.
[36] H. Tian, Y. Shu, X. F. Wang, M. A. Mohammad, Z. Bie, Q. Y. Xie, C. Li, W. T. Mi, Y. Yang, T. L. Ren, *Sci. Rep.* **2015**, *5*, 8603.
[37] S. Pyo, J. Lee, W. Kim, E. Jo, J. Kim, *Adv. Funct. Mater.* **2019**, *29*, 1902484.
[38] M. Chen, X. Hu, K. Li, J. Sun, Z. Liu, B. An, X. Zhou, Z. Liu, *Carbon N. Y.* **2020**, *164*, 111.
[39] B. Zhu, Z. Niu, H. Wang, W. R. Leow, H. Wang, Y. Li, L. Zheng, J. Wei, F. Huo, X. Chen, *Small* **2014**, *10*, 3625.
[40] G. Y. Bae, S. W. Pak, D. Kim, G. Lee, D. H. Kim, Y. Chung, K. Cho, *Adv. Mater.* **2016**, *28*, 5300.
[41] Z. Wang, X. Guan, H. Huang, H. Wang, W. Lin, Z. Peng, *Adv. Funct. Mater.* **2019**, *29*, 1807569.
[42] Z. Chu, W. Jiao, Y. Huang, Y. Zheng, R. Wang, X. He, *J. Mater. Chem. A* **2021**, *9*, 9634.
[43] K. K. Kim, S. Hong, H. M. Cho, J. Lee, Y. D. Suh, J. Ham, S. H. Ko, *Nano Lett.* **2015**, *15*, 5240.
[44] T. H. Chang, Y. Tian, D. L. Y. Wee, H. Ren, P. Y. Chen, *Small* **2018**, *14*, 1800596.
[45] C. Cao, Y. Zhou, S. Ubnoske, J. Zang, Y. Cao, P. Henry, C. B. Parker, J. T. Glass, *Adv. Energy Mater.* **2019**, *9*, 1900618.
[46] C. Cao, H. F. Chan, J. Zang, K. W. Leong, X. Zhao, *Adv. Mater.* **2014**, *26*, 1763.
[47] J. Zang, S. Ryu, N. Pugno, Q. Wang, Q. Tu, M. J. Buehler, X. Zhao, *Nat. Mater.* **2013**, *12*, 321.

[48] S. Zhang, L. Wen, H. Wang, K. Zhu, M. Zhang, *J. Mater. Chem. C* **2018**, *6*, 5132.
[49] M. De Volder, S. H. Tawfick, S. J. Park, D. Copic, Z. Zhao, W. Lu, A. J. Hart, *Adv. Mater.* **2010**, *22*, 4384.
[50] H. Niu, S. Gao, W. Yue, Y. Li, W. Zhou, H. Liu, *Small* **2020**, *16*, 1904774.
[51] Y. Xiong, Y. Shen, L. Tian, Y. Hu, P. Zhu, R. Sun, C. P. Wong, *Nano Energy* **2020**, *70*, 104436.
[52] B. He, Z. Yan, Y. Zhou, J. Zhou, Q. Wang, Z. Wang, *J. Micromech. Microeng.* **2018**, *28*, 105001.
[53] K. Sim, Z. Rao, Z. Zou, F. Ershad, J. Lei, A. Thukral, J. Chen, Q. A. Huang, J. Xiao, C. Yu, *Sci. Adv.* **2019**, *5*, eaav9653.
[54] D. Lee, H. Lee, Y. Jeong, Y. Ahn, G. Nam, Y. Lee, *Adv. Mater.* **2016**, *28*, 9364.
[55] J. Qiu, X. Guo, R. Chu, S. Wang, W. Zeng, L. Qu, Y. Zhao, F. Yan, G. Xing, *ACS Appl. Mater. Interfaces* **2019**, *11*, 40716.
[56] J. Lee, S. Pyo, D. S. Kwon, E. Jo, W. Kim, J. Kim, *Small* **2019**, *15*, 1805120.
[57] T. H. Chang, Y. Tian, C. Li, X. Gu, K. Li, H. Yang, P. Sanghani, C. M. Lim, H. Ren, P. Y. Chen, *ACS Appl. Mater. Interfaces* **2019**, *11*, 10226.
[58] X. Yu, Z. Xie, Y. Yu, J. Lee, A. Vazquez-Guardado, H. Luan, J. Ruban, X. Ning, A. Akhtar, D. Li, B. Ji, Y. Liu, R. Sun, J. Cao, Q. Huo, Y. Zhong, C. M. Lee, S. Y. Kim, P. Gutruf, C. Zhang, Y. Xue, Q. Guo, A. Chempakasseril, P. Tian, W. Lu, J. Y. Jeong, Y. J. Yu, J. Cornman, C. S. Tan, B. H. Kim, K. H. Lee, X. Feng, Y. Huang, J. A. Rogers, *Nature* **2019**, *575*, 473.
[59] M. F. L. De Volder, S. J. Park, S. H. Tawfick, D. O. Vidaud, A. J. Hart, *J. Micromech. Microeng.* **2011**, *21*, 045033.